Halloysite Nanotubes and Metal Corrosion Inhibitors: a Computational and Experimental Study

Riccardo Rozza,[†] Nerina Armata,[†] Giuseppe Lazzara,[†,‡] Filippo Parisi,[†] and Francesco Ferrante[*,†]

[†]*Università degli Studi di Palermo - Dipartimento di Fisica e Chimica, Viale delle Scienze Ed. 17, 90128 Palermo, Italy*

[‡]*Consorzio Interuniversitario Nazionale per la Scienza e Tecnologia dei Materiali, INSTM, Via G. Giusti, 9, I-50121 Firenze, Italy*

E-mail: francesco.ferrante@unipa.it

Phone: +39 091 23897979. Fax: +39 091 590015

Abstract

Halloysite nanotubes are widely used as a substrate for the controlled release of various types of molecules in an increasing number of applications. In this work, the interactions of halloysite silicic and aluminic surfaces with corrosion inhibitors compounds, such as benzotriazole, 8-hydroxyquinoline, 2-mercaptobenzimidazole and 2-mercaptobenzothiazole, were investigated from a computational point of view. Two new halloysite compounds with salicylaldoxime and quinaldic acid were designed. Here we propose their synthesis, evaluate amounts of loading and analyse the adsorption behaviour.

Introduction

One of the most active current research topics in metallurgic industry involves the design of innovative compounds, which avoid the permeation of corrosive substances on metal manufacts.[1,2] In the past, the most common method was the use of Cr^{6+} that, being toxic and carcinogen, was banned in 2007 in Europe.[3] It was therefore necessary to find less dangerous ways to protect metal surfaces. One of the best options has been the passivation of desired areas by covering them with an organic inhibitor thin film. Polymers and sol-gel coatings are commonly used, but their application is ineffective when small fractures are present.[4] In this context, recent studies are aimed at the identification of composite materials in which the corrosion inhibitor molecule is trapped in a matrix or substrate, so that it can be released in a controlled way, giving a self-healing process.[5] The perfect passivation anti-corrosion agent should form stable complex with the metal components as soon as they come in contact. In this respect, organic compounds with nitrogen or sulfur atom or chelant portion in their structure seem to be perfect candidates. For example, benzotriazole,[6] mercaptobenzothiazole,[7] mercaptobenzimidazole,[8] salicylaldoxime, 8-hydroxyquinoline,[9,10] and quinaldic acid[11] have shown high efficiency in inhibiting corrosion processes. They also tend to enhance their performance when used as nanocomposite materials with an appropriate substrate or encapsulad in a polymeric matrix.[12,13]

Among the materials used as substrates, halloysite nanotubes (HNT) play a prominent role thanks to their special chemical-physical properties.[14–16] It is suitable for industrial application, since it is inexpensive but also environmental friendly and non-toxic.[16–18] Halloysite is a mineral belonging to the kaolinite family and it is present in nature mainly in the form of nanoscrolls with characteristic sizes and properties that are dependent on the deposit.[19,20] From a stuctural point of view it is made up by a layer of tetrahedral silicon connected to an octahedral aluminium layer which, during the spiralization process, undergoes distortions whose nature and origin are still under discussion.[21,22] Its particular tubular form and surface chemistry allows targeted modifications and the inclusion of a wide range

of small molecules, as the organic corrosion inhibitors, for a slow and controlled release.[23–26]

Lvov et al. developed nanocomposites in which benzotriazole (BT), 8-hydroxyquinoline (IQ), mercaptobenzimidazole (MBI) and 2-mercaptobenzothiazole (MBT), trapped within the halloysite nanotube lumen, were used as efficient corrosion inhibitors for bronze, steel, copper and aluminum.[11,23,27,28] The inclusion ensures that inhibitors are not washed away neither react with other species before forming the complex with the metal to be preserved. Morevoer, the release can be tuned by using nanotube end stoppers, so that small concentrations of anti-corrosives is required in order to create lasting protective films.[29,30]

In this work we focused on the adsorption process of organic corrosion inhibitors BT, IQ, MBI and MBT on halloysite surfaces. As stated before, their efficiency is well documented. Nevertheless, there is no clear view on adsorption atomistic details and their correlation with loading capacity. A computational study on these systems provides a better understanding of these processes. Thus, adsorption geometries and energies were computed and the leading surface-adsorbate interactions evaluated. Acquired information were employed to design two new halloysite nanocompounds: between common organic corrosion inhibitors, salicylaldoxime (SA) and quinaldic acid (QA) were identified as potential candidate. While a lot of experimental data are available for most of the aforementioned molecules, there is no information on SA and QA loading capacity and their adsorbtion behaviour. These properties were evaluated in this work by means of thermogravimetric analysis (which allows to determine the weight percentage of organic compounds adsorbed onto clay), UV-Vis Spectroscopy and Differential Scanning Calorimetry. Moreover, the interpretation of the obtained results provides useful information about the mechanism of adsorption of the two species related to the adsorbate/substrate and adsorbate/adsorbate interactions.

Computational Details and Models

All calculations were performed at density functional theory level, by using the Gaussian 09 software.[31] The M06L metaGGA exchange-correlation functional[32] was joined with the Ahlrichs and co-workers valence double zeta plus polarization basis set for all calculations.[33–35] The M06L functional allows to describe in a reliable way the dispersion interactions in the study of molecular adsorption on surfaces; it was preferred to the M06-2X one because it allows to efficiently exploit the resolution of identity approximation, helpful for treating systems of large dimensions. The split valence plus polarization (VZP) basis set employed has the following contraction schemes: H (4s1p)/[2s1p]; C, O, N (7s4p1d)/[3s2p1d]; Al, Si, S (10s7p1d)/[4s3p1d]. The auxiliary functions corresponding to VZP basis set were used for RI approximation.

The halloysite portion used in this modelling study has the stoichiometric formula $H_{48}Al_{24}Si_{24}O_{126}$ and is showed in Figure 1. It was cropped from a model halloysite nanotube, with a 5 nm diameter, previously constructed and characterized computationally by means of density functional tight binding theory.[36] Hydrogen atoms were used to saturate the dangling bonds originated from the cutting; we have already proved that this artefact does not affect the general conclusion regarding the investigation of small molecules adsorption. As a a matter of fact, the same computational model was adopted in a previous case, to which we refer for its structural details.[37] In order to stress the importance of a curved surface model we must take into account that, according to our previous computational studies on the halloysite nanotube,[36] the spiralization of the kaolinite sheet leads to an increase of 0.3 and 0.1Å, in the mean, of the distance between two opposite vertexes of the Si and Al surface hexagonal arrangements, respectively. The distortions, that are not negligible, could give rise to slight differences on the molecules adsorption geometries, hence on interaction energies, if compared with the adsorption process on a flat surface.

In this study, the adsorbate-halloysite interaction energies, ΔE_{ads}, corrected for the basis set superposition error estimated by means of the counterpoise procedure,[38] were computed

as the difference between the energy of the whole aggregate and the energies of the isolated constituents.

[Figure 1 about here.]

Materials and Experimental Methods

Materials

Quinaldic acid, salicylaldoxime and halloysite nanotubes with a specific gravity of 2.53 g cm^{-3} and a specific surface area of 65 m^2 g^{-1} are from Sigma-Aldrich (Milan, Italy). All chemicals were used without further purification. The hybrid materials were prepared by mixing the organic compound with the HNT water dispersion at room temperature. Afterwards, the obtained dispersions were stirred magnetically overnight followed by sonication treatment for 15 min and kept under vacuum 1 hour. The procedure was repeated two times to maximise the loading of compounds. After centrifugation the supernatant was removed by centrifugation. The so obtained compounds were dried in oven at 50°C.

Experimental Methods

Thermogravimetric Analysis (TGA): The experiments were done by using the Q5000 IR (TA Instruments) under nitrogen flow (25 cm^3 min^{-1}) by heating the samples from room temperature to 700°C. Each sample (ca. 8 mg) was placed in a high temperature platinum pan and heated under a temperature ramp of 20°C min^{-1}. Loading was calculated by applying the "rule of mixtures" according to the procedure in the literature.[39,40]

Differential Scanning Calorimetry (DSC): The differential scanning calorimeter Ta Instruments 2920 CE was used. The apparatus was calibrated with indium.[41] The aluminium pans were filled with ca. 6 mg of the compound. The measurements were carried out by cooling the sample to -10°C at -10°C/min and heating from -10°C to 180°C at 10°C/min. The

baseline was subtracted according to the literature.[42] In order to construct the adsorbtion isotherms, the solution were prepared by adding appropriate aliquots of the organic compounds to the HNT dispersion at room temperature. Afterwards, the obtained dispersions were stirred magnetically overnight followed by sonication treatment for 15 min and kept under vacuum by using continuously a vacuum pump for 1 hour. The procedure was repeated two times to ensure equilibration. After centrifugation the supernatant was removed. The gathered supernatants were spectrophotometrically analyzed in order to construct the adsorption isotherms. In particular the spectral absorbance of the aqueous solutions were registered at 258 nm for Salicylaldoxime and at 320 nm for Quinaldic acid with a diode-array Analytic Jena S600 spectrophotometer equipped with thermostated compartments for 1×1×5 cm cuvettes and an appropriate magnetic stirring apparatus. In order to study the release kinetics a portion of both composites were placed in a quartz cuvette to register the slow release of the active compounds from the composites. The release were followed for ca. 24 hours.

Discussion

Computational results

Self-healing materials are widely used and appreciated by industrial and scientific communities. In order to achieve the desired properties, one crucial point in smart material design relies on the comprehension of the substrate-adsorbate interactions. Here we examine the structure of the selected organic corrosion inhibitors and how they adsorb on silicic and aluminic halloysite surfaces. The structure of the considered molecules can roughly be divided in two portions: i) an interacting part containing O, S, N and H atoms, responsible of hydrogen bonds formation and ii) an aromatic part, which can give rise to π interactions with the surface.

As starting point for geometry optimization, parallel and perpendicular orientations, with

respect to the silicic or aluminic halloysite surface, were considered for all the investigated anti-corrosion compounds. In the following, the term "parallel (perpendicular) orientation" will be used also to indicate the optimized geometry of the system resulting from the corresponding starting point, even if the geomeries did not maintain the original orientations. The adsorbates were initially located at the center of the halloysite model, both on silicic and on aluminic surface. After geometry optimization, they retain positions largely distant from the edges, confirming that the portion of nanotube employed is large enough to describe the adsorption.

The most representative molecular conformations of IQ, MBI, MBT, QA and SA were taken into account, in order to see if effective interactions with halloysite surfaces can occur with the retaining of the intramolecular hydrogen bond, where present. These conformations are depicted in Figure 2, together with the atom numbering scheme used throughout and their relative energies.

[Figure 2 about here.]

In the following, hydrogen bonds will be described by means of two geometrical parameters: the H-bond distance (r, in Angstroms) and the X$\hat{\text{H}}$Y angle (a, in degrees), with X,Y = O, N, S. To avoid redundancy in writing the short notation XHY(r,a) will be used throughout, being the atom center belonging to the halloysitic system always on the right; a dash on the left (right) of H will indicate wheter the halloysite surface acts as donor (acceptor) of the H-bond. The notation XHY(r_1,a_1/r_2,a_2) will indicate a bridge hydrogen bond. Hydrogen bonds with distance larger than 3 Å and X$\hat{\text{H}}$Y angle outside the 140-180° range were considered as secondary interactions and, even though they could have some relevance in determining the adsorption geometry, they will not be generally described in details. In order to analize the results on the energetics of the adsorption, it will be enlightening to know that, with the calculation method employed in this work, a BSSE-corrected interaction energy of 16.2 kJ mol^{-1} was estimated for the benzene molecule adsorbed on the silicic surface, being the interaction solely due to van der Waals contributions involving the π cloud.

The calculated interaction energies of the investigated compounds (in various conformations and orientations) with the halloysite silicic and aluminic surfaces are collected in Tables 1 and 2. These results will be discussed in the following sections, along with the adsorption geometries.

[Table 1 about here.]

[Table 2 about here.]

Benzotriazole

Benzotriazole weakly interacts with silicic surface: adsorption energies of -23.2 and -20.4 kJ mol^{-1} for parallel and perpendicular orientations were estimated. The small energy difference between the two adsorption geometries is likely due to a slight preference for a spreader van der Waals π interaction in the former rather than a more directional H-bond with silicic surface. Once adsorbed, BT is unable to form a strong hydrogen bond as donor, as suggested by the interaction NH-O(2.854, 138) in parallel orientation, see Figure 3a. Perpendicular BT does not form any H-bond with oxygen atoms from the surface. Its adsorption energy could be ascribed to weak van der Waals interactions.

On aluminic layer, the parallel and perpendicular orientations of the adsorbate show the same type of interactions: NH-O is the main one, with NH-O(1.734, 155) and NH-O(1.664, 167), respectively; a bridged H-bond is present in both orientations, with geometry N_2-HO(2.120, 142/2.333, 143) and N_2-HO(2.199, 158/2.147, 152). Parallel and perpendicular BT show adsorption energy ΔE_{ads} of -59.5 and -62.3 kJ mol^{-1}, respectively. This values are fairly high for a molecule without any oxygen atoms. The small adsorption energy difference between the two orientations is likely due to the presence of a better oriented and more symmetric double H-bond in perpendicular case, showed in Figure 3b. In conclusion, the results collected suggest that benzotriazole energetically prefers the adsorption on halloysite inner lumen.

[Figure 3 about here.]

8-Hydroxyquinoline

The 8-hydroxyquinoline molecule has two chemical sites relevant for the adsorption process: the piridinic nitrogen atom and the hydroxyl group. Two possible IQ conformations of interest were identified: the first, IQa, is the one without the intramolecular hydrogen bond, which in contrast is present in IQb. Isolated IQb is 36.2 kJ mol^{-1} more stable than IQa.

On silicic surface, we computed ΔE_{ads} of -25.5 and -21.5 kJ mol^{-1} for parallel and perpendicular IQa and ΔE_{ads} of -24.4 and -13.0 kJ mol^{-1} for parallel and perpendicular IQb. Like in BT case, in parallel orientation of both IQa and IQb the small adsorption energy is due to the exclusive presence of van der Waals interactions. Conversely, perpendicular IQa and IQb are able to form an H-bond with a surface oxygen, having geometry OH-O(2.111, 161) and OH-O(3.007, 163), respectively. The adsorption energy of IQa is nearly 60% larger than that of IQb. Nevertheless, IQa is the less stable conformation in vacuum and its formation from IQb would require more energy than that gained by adsorption, resulting in an endoergic process. This would prevent IQa from being the the conformation present on the halloysite silicic surface and therefore the direct adsorption of IQb in parallel orientation (Figure 4a) is preferred.

On aluminic surface, ΔE_{ads} as large as -72.4 and -78.5 kJ mol^{-1} were computed for parallel and perpendicular IQa, and ΔE_{ads} of -37.4 and -56.4 kJ mol^{-1} for parallel and perpendicular IQb. Actually, the optimized geometries of IQa in the two orientations are not too different: IQa is always almost parallel to the surface and the interactions can be listed as: a single H-bond OH-O(1.928, 148) plus two double H-bonds O-HO(3.066, 146/2.060, 136) and N-HO(2.730, 133/2.384, 139) for parallel IQa; two single H-bonds OH-O(1.747, 156), O-HO(2.004, 136) plus a double H-bond N-HO(2.770, 149/2.167, 170) for perpendicular IQa. The high adsorption energy values are due to the these extended H-bond network. Even if parallel IQa has a further secondary interaction with the same hydrogen atom involved in

H-bond with hydroxyl group, perpendicular IQa is a little bit more stabilized. In this case the quality, and not the amount, of the interactions is discriminant in lowering the system energy: H-bonds of perpendicular orientation are generally shorter and better oriented than parallel ones. In parallel IQb the H atom from hydroxyl group cannot form H-bonds as donor, thus only two H-bonds as acceptor from oxygen and nitrogen atom were revealed. This fact is mirrored in the interaction energy, ca. 52% smaller with respect to IQa. Despite the retaining of intramolecular H-bond, perpendicular IQb forms an extensive H-bond network that lowers the system energy more than in parallel case: a double N-HO(2.321, 157/2.430, 143), a further double O-HO(2.238, 154/2.496, 150) and a single OH-O(1.662, 147). These interactions result in an interaction energy of ca. 66% stronger that that of the parallel IQb, which is able to form only two H-bond as acceptor with the oxygen O-HO(2.063, 176) and nitrogen atoms N-HO(2.416, 152). However, despite the stronger global interaction of IQa with halloysite, if the energy for the IQb to IQa conversion is taken into account, the direct adsorption of IQb (the most stable geometry is shown in Figure 4b) is again the preferred choice, being the most exoergic process.

[Figure 4 about here.]

2-Mercaptobenzimidazole and 2-Mercaptobenzothiazole

Two conformations of MBI were considered, one in which the hydrogen atom of the SH group is on the opposite side of the one linked to N_1 (MBIa) and another one in which they are on the same side (MBIb). The latter is 10.9 kJ mol^{-1} more stable than the former.

On silicic surface, ΔE_{ads} of -33.6 and -38.9 kJ mol^{-1} for parallel and perpendicular MBIa and of -10.8 and -21.6 kJ mol^{-1} for parallel and perpendicular MBIb have been calculated. In the most stable geometry, MBIa is placed parallel to the silicic surface with the center of its imidazole moiety located just atop an oxygen atom, as showed in Figure 5a. On inner halloysite surface, ΔE_{ads} are -67.6 and -92.5 kJ mol^{-1} for parallel and perpendicular MBIa. This last orientation of MBIa gives rise to a double N-HO(2.025, 172/2.453, 167)

and a single SH-O(1.656, 178) and is the most stable form of 2-mercaptobenzimidazole on halloysite (Figure 5b), while parallel MBIa forms one H-bond with its thiolic portion both as donor, SH-O(1.867, 157), and as acceptor, S-HO(2.480, 146), and a further N-HO(2.205, 150). On the other hand, adsorption energies of -46.2 and -58.1 kJ mol^{-1} were evaluated for parallel and perpendicular orientations of MBIb. In parallel MBIb the thiolic hydrogen atom points toward the center of the model, thus donor-acceptor interactions are no longer possible. The only H atom available for the interaction is the nitrogen one, that forms N-HO(2.267, 156). In perpendicular orientation, MBIb has lower adsorption energy than MBIa: in this geometry MBIb forms two H-bonds, SH-O(2.037, 161) and NH-O(1.735, 175), so a double H-bond as acceptor is replaced by a single H-bond as donor. The directional H-bonding on aluminic surface appears therefore to be the driving force in the adsorption of 2-mercaptobenzoimidazole. On both silicic and aluminic surfaces, the difference in interaction energies overcome the small energy required for the conversion from MBIb to MBIa, and the MBIa form is energetically preferred when adsorbed.

[Figure 5 about here.]

In the two possible conformations of mercaptobenzothiazole (MBTa and MBTb), the thiolic hydrogen atom points toward the nitrogen atom and toward the sulphur one, respectively, being only +4.3 kJ mol^{-1} the MBTa-MBTb energy difference.

Adsorption geometries of parallel and perpendicular MBT on silicic surface are very similar to that of MBI. We observed long range interactions and calculated small ΔE_{ads}: -26.8 and -30.8 kJ mol^{-1} for parallel and perpendicular MBTa, and -21.7 and -21.0 kJ mol^{-1} in the MBTb case. There is no clear distinction between the two orientations when we look at optimized geometries. Non-directional π interactions seem to be the major contributions to the adsorption energies thus, very like mercaptobenzimidazole, MBT lies parallel to the silicic surface (see Figure 6a).

On aluminic surface, ΔE_{ads} amount to -55.1 and -74.0 kJ mol^{-1} for parallel and perpendicular MBTa and to -44.6 and -38.9 kJ mol^{-1} for parallel and perpendicular MBTb. Parallel

MBT(a and b, in order) both form one weak H-bond involving the thiolic group, SH-O(1.834, 157) and SH-O(1.739, 167). Energy differences can be explained by considering the different interactions as hydrogen bond acceptor. In MBTa a double N-HO(2.189, 160/2.665, 162) exists, while in MBTb two separate H-bonds were revealed, one S-HO(2.442, 177) and one N-HO(2.315, 143). Perpendicular MBT(a,b) lie in a similar manner on aluminic surface. They both give rise to an H-bond as donor with thiolic portion: SH-O(1.669, 175) and SH-O(1.819, 172), in order for MBTa and MBTb conformations. Nevertheless, their interaction energies differ by 35.1 kJ mol^{-1} in favour of MBTa. This is not surprising, since the H-bond double acceptor is the nitrogen atom in MBTa and the sulfur one in MBTb. In details, perpendicular MBTa shows a N-HO(2.105, 175/2.649, 163), while MBTb has an S-HO(2.419, 152/2.626, 155). The most stable geometry of MBT on aluminic surface is showed in Figure 6b.

Analogously to the MBI case, adsorption of MBTa is the most exoergic process on both surfaces, considering the low energy difference for MBTb to MBTa conversion.

[Figure 6 about here.]

Quinaldic acid

Quinaldic acid has two chemically relevant sites: the piridinic portion and the carboxylic group in ortho position with respect to the heteroatom. An intramolecular H-bond can exist between nitrogen atom and carboxylic OH. Three possible conformations of interest were identified: in the first, QAa, there is no intramolecular H-bond and the C=O group points on the same side of N atom; in the second, QAb, there is the intramolecular H-bond, so the -OH portion looks towards N atom; the third, QAc, is similar to QAb but the -OH moiety points away from N atom (no intramolecular H-bond). QAb is the most stable conformation, followed by QAc (+15.9 kJ mol^{-1}) and QAa (+23.0 kJ mol^{-1}).

Quinaldic acid weakly interacts with silicic surface. In parallel orientation, the main contributions for all three conformations reside in van der Waals interactions, since the H-bonds

geometric parameters are well outside the appropriate angular ranges: they are H-OH(2.387, 117), H-OH(2.687, 99) and H-OH(2.467, 107) for parallel a, b and c conformations, respectively. As expected in absence of a peculiar interaction, the adsorption energies are small and comparable with each other: -26.6, -31.6 and -28.3 kJ mol^{-1} for QAa, QAb and QAc. Retaining the intramolecular H-bond in QA adsorption geometry is more advantageous than forming H-bond with silicic surface, i.e. the energy difference between QAb and the other two conformations makes parallel QAb the most stable adsorption geometry. Calculated adsorption energies for perpendicular QA are -22.2, -11.8 and -16.8 kJ mol^{-1} for a, b and c conformations, respectively. It appears clear that the loss of the main interaction in QAb, which forms a weak H-bond as acceptor with the hydrogen from halloysite interlayer, with O-HO$_{il}$(2.791, 131), raises the system energy. QAa and QAc form H-bonds both as donor and acceptor: as donor OH-O(1.924, 162) and OH-O(1.876, 165) were found for QAa and QAc, respectively; as acceptor, the hydrogen from interlayer is involved, being O-HO$_{il}$(1.979, 159) and O-HO$_{il}$(2.271, 153) for QAa and QAc, respectively. Adsorption energies differences for a and c conformations may be due to more extended van der Waals interactions from the remaining part of the adsorbate in QAa with respect to QAc. Therefore, on silicic surface parallel QAb shows the highest interaction energy (Figure 7a).

As found for all the systems investigated in this work, stronger adsorption energies were calculated on aluminic surface. Thanks to the carboxylic functional group and the nitrogen atom in the piridinic ring, QA is able to form several H-bonds with halloysite. The van der Waals interactions involving the aromatic portion help the purpose of lowering the system energy, especially when parallel adsorption geometries are considered. Interaction energies of -99.0, -69.8 and -77.9 kJ mol^{-1} were found for parallel QA in a, b and c conformations, respectively. All of them have the chance to form H-bond as acceptor with the nitrogen atom: these are described as N-HO(2.316, 147), N-HO(2.179, 154/2.980, 150)) and N-HO(2.519, 142) for QAa, QAb and QAc. Additionally, the three conformations give rise to H-bonds by acting both as donor and acceptor involving the O-containing moieties. In details, for

QAa: N-HO(2.316, 147), OH-O(1.879, 153) and O-HO(1.773, 162); for QAb O-HO(1.949, 156), OH-O(1.2.478, 128) and O-HO(2.056, 142) with HO outside the central ring; for QAc: N-HO(2.519, 142), OH-O(1.771, 146) and O-HO(2.026, 153). Considering the differences in conformation energy, the final adsorption esoergicity order is QAa > QAb > QAc for parallel geometries.

Perpendicular orientation of QA on aluminic surface results in ΔE_{ads} of -80.0, -76.4 and -99.0 kJ mol^{-1} for a, b and c conformations, respectively. Optimization of a perpendicular starting geometry ends with an almost parallel one for QA(b,c). In details: QAb forms O-HO(2.026, 150) and a further double H-bond as acceptor with its -C=O portion, O-HO(2.092, 161/2.114, 158); QAc forms OH-O(1.711, 153), O-HO(1.963, 152) and a further N-HO(2.201, 149). QAa is the only one with a nearly perpendicular equilibrium geometry. It gives raise to a OH-O(1.562, 175) and a double O-HO(1.942, 164/2.090, 154). This latter interaction counterbalances the loss of the secondary nitrogen H-bond interaction (too distant from surface). As a consequence the ΔE_{ads} is similar to the parallel case. Energy differences respect to the latter in QAb are likely due to the double H-bond: it involves the nitrogen atom in parallel QA (while oxygen atom forms a single H-bond) and the oxygen atom in perpendicular QA (while nitrogen atom is not involved in forming any bond). In QAc case, the adsorption energies of the perpendicular orientation is higher than that of parallel one: the energy minimum is reached by involving a closer interaction with the nitrogen atom. Comparing the results for QAc and QAb, it seems that the retaining of intramolecular H-bond is less favourable with respect to the interaction with -OH aluminic portion. In perpendicular conformation, therefore, an inversion in the stability order is observed when conformation energy differences are considered: QAa results less stable than QAb but the perpendicular adsorption of QAc (with the geometry showed in figure 7b) gives raise to the most exoergic process.

[Figure 7 about here.]

Salicylaldoxime

The salicylaldoxime molecule has an oxime group (RH)-C=N-OH and a phenolic group both able to form hydrogen bonds with the surfaces. As regards the two relevant conformations, the absence of the intramolecular H-bond in SAa makes it +42.6 kJ mol^{-1} less stable than SAb.

On silicic surface, parallel and perpendicular SAb show only a H-bond with a surface oxygen atom, OH-O(2.390, 115), to be considered as secondary interaction, and OH-O(2.058, 147), respectively. Computed adsorption energies are -26.2 and -13.0 kJ mol^{-1}. On the other hand, parallel SAa forms a double H-bond as donor with its phenolic group, both identifiable as secondary interactions, while perpendicular SAa forms a double H-bond with its oxime portion using two different oxygen atoms of the surface: OH-O(2.196, 145/2.591, 146). Calculated adsorption energies are -28.2 and -23.0 kJ mol^{-1} for parallel and perpendicular SAa. For parallel geometry, the spreader π interactions leads to a more pronounced energy gain with respect to the exclusive directional H-bond ones of the perpendicular configuration. Nevertheless, looking at the mere adsorption process, the H-bond interaction with silicic surface is more energetically advantageous than the retention of the intramolecular one. This fact would lead the parallel SAa conformation to be the most stable adsorption geometry. The stability order is reversed when the energy difference between the SAa and SAb conformations is considered. In this case, SAa adsorption energy turns from negative to positive (+14.4 and +19.6 kJ mol^{-1} for parallel and perpendicular SAa). Thus energy gain from adsorption on silicic surface is not enough to overcome the one required for the conformation change. The most stable adsorption geometry (parallel SAb) is showed in Figure 8a.

On aluminic surface, salicylaldoxime shows a much more pronounced adsorption energy. As a matter of fact, ΔE_{ads} values of -54.1 and -69.9 kJ mol^{-1} for parallel and perpendicular SAb and of -110.1 and -117.3 kJ mol^{-1} for parallel and perpendicular SAa were estimated. This energy difference between the two surfaces is due to the particular salicylaldoxime

structure: on the aluminic layer, the SA forms a larger number of H-bond both as donor and acceptor. A similar argumentation is the key to understand the difference between a and b conformations. In the latter, the intramolecular H-bond deprives SA of a further interaction, thus inhibiting the adsorbate to maximize the number of surface binding. On the inner surface, parallel and perpendicular SAb converge into similar adsorption geometries. They differ only for the presence of one donor-acceptor double H-bond (aldoxime portion) in parallel orientation and a closer intramolecular H-bond in perpendicular orientation. This latter interaction stabilizes SAb more than a further H-bond as acceptor with surface, thus perpendicular SAb shows a larger adsorption energy. In details, parallel SAb gives rise to one O_{oxime}H-O(1.804, 163), plus one O-HO(1.868, 165) and a further $O_{hydroxyl}$-HO(1.952, 162); at variance, perpendicular SAb forms O_{oxime}H-O(1.798, 158), plus a O-HO(2.603, 173).

Like the SAb case, also parallel and perpendicular SAa show similar adsorption geometries (the most stable is reported in Figure 8b). Listed in order, there are two H-bonds as donor: one with aldoxime portion OH-O(1.705, 158) and OH-O(1.712, 159) and another with hydroxyl portion OH-O(1.618, 161) and OH-O(1.617, 160); they also present N-HO(2.157, 156) and N-HO(2.100, 157) bindings. Unlike the adsorption process on silic surface, herein the stability order remains unaffected even considering conformation energy difference. Parallel and perpendicular SAa adsorption energies turn into -67.5 and -74.4 kJ mol^{-1} if the energy for conformation change is taken into account.

[Figure 8 about here.]

Experimental results

Computational results suggest that composites based on QA and SA with HNT could be efficient as carrier for anti-corrosion agent. Nevertheless, confirmation from experimental analysis are required in order to enforce this hypothesis.

Thermogravimetric Analysis

The thermogravimetric curves showed in Figure 9 were normalized at 150°C for the adsorbed water to visualize the different loadings of the organic compounds. TGA curves for HNTs presents multistep mass loss due to different kind of bound water and dehydroxylation on the alumina surface at larger temperature. These features have been deeply discussed in literature.[43] The amount of corrosion inhibitors loaded on the HNTs was estimated on the residuals at 700°C by using the rule of mixtures.[44] The thermograms show 0.6 wt% of loading for SA and 4.8 wt% for QA. According to the geometrical calculations performed by Cavallaro et al.[45] these data suggest just a monolayer formation on HNT surface for the SA and a multilayer for QA. In this case, the loading efficiencies of the QA on the HNT is eight times bigger that SA ones. The intermolecular affinity of the QA molecules with themselves respect to the affinity of SA ones could play a fundamental role in adsorption process. In order to confirm this hypothesis, DSC analysis and UV-Vis Spectroscopy were performed.

[Figure 9 about here.]

Differential Scanning Calorimetry

From DSC measurements (Figure 10), melting temperature (T_m) of 59.5°C and 159.5°C were obtained for SA and QA, respectively. The corresponding enthalpy of melting for SA and QA are 133 and 192 J g^{-1}, respectively, showing stronger intermolecular interactions occurring in QA. As far as the HNT loaded systems, a straightforward decrease of crystallinity is observed in both composites. In particular, the HNT/QA mixture shows a melting enthalpy of only 1.04 J/g indicating a residual crystallinity of ca. 11% among the all QA mass in the composite. Moreover, the HNT/SA composite did not give any detectable signal due to a negligible residual crystallinity. On this basis one can argue that the interaction with the HNT surface disturbs the crystallization of the organic substances and that only for the system featuring a multilayer adsorption (QA) a residual crystallinity is observed. On the other hand the computational analysis suggested that the adsorption has a profound effect

on the stable conformation of QA and SA with large influence on intramolecular hydrogen bonding, that likely also influences the crystallization/melting process.

[Figure 10 about here.]

UV-Vis Spectroscopy

The different adsorption behaviour of the two species was confirmed by constructing the adsorption isotherms (Figure 11) at 25°C, where the equilibrium amount of organic component adsorbed onto the clay (C_s, mg g^{-1}) is plotted as a function of the equilibrium concentration in solution (C_e, g dm^{-3}). It is clearly evidenced that, according to TGA results, the amount of QA adsorbed onto HNT is much higher than that of SA.

[Figure 11 about here.]

Among the different models, the Freundlich isotherm revealed as the most reliable in reproducing the experimental data for both QA and SA. Notably, the model accounts for intermolecular interactions between adsorbates[46] and implies heterogeneity of adsorption sites and/or formation of multilayers.[47–52] The Freundlich isotherm, is described by the equation:

$$C_s = K_F C_e^{1/n}$$

where K_F is the Freundlich adsorption coefficient or capacity factor, which represents the adsorption capacity of the clay, and n is a dimensionless adsorption intensity constant, which is a measure of the adsorption intensity. The obtained fitting parameters are collected in Table 3.

[Table 3 about here.]

Even if the use of different units makes the obtained values of the adsorption capacity K_F not rigorously comparable,[53] the very significant differences observed in the K_F and in the

adsorption isotherms shown in Figure 11 confirms the hypothesis of stronger solute/solute interactions, which favour the formation of multilayers. On the other hand, the values of the intensity factor (n) are comparable for the two species, thus indicating very similar clay/solute interactions. In other words, the different percentage of loaded amount obtained from TGA measurements can be attributed to the strong effect of the intermolecular interactions, which are more significant for the quinaldic acid, due to its higher polarity.

As regards the ability of the corrosion inhibitors to be released from the HNTs compounds and delivered to their site of action we performed release kinetics experiments for both composites (SA/HNT and QA/HNT). A certain amount of composites was placed in water and adsorption spectra were registered as function of time as shown in Figure 12. The diagram clearly shows a prompt release of the compounds from the HNTs in the first 2 hours. Afterwards a net difference in the release velocity is visible between the two composites. After 10 hours, while ca. 90% of the payload is released for SA/HNT, just 20% of the loaded compound is released for QA/HNT. This large difference can be interpreted by considering that the drug release for QA/HNT is likely due to the breakage of the interactions between drugs molecules (QA-QA interaction). As regards SA/HNT composite weaker interactions between HNT and SA have to be taken into account. Furthermore, these explanations are in agreement with our finding that a monolayer of SA is adsorbed on the Halloysite in SA/HNT and multilayers of QA on the QA/HNT. According to these results, in both cases HNTs can be considered suitable carriers of these active species.

[Figure 12 about here.]

Conclusion

The adsorption geometries and energetics of six molecules, effective as metal corrosion inhibitors, on the silicic and aluminic surfaces of a halloysite nanotube model was investigated by means of density functional theory. Based on the calculated interaction energies, all in-

vestigated molecules largely prefer to adsorb in the inner cavity surface of the nanotube, by exploiting the possibility of forming a stable network of hydrogen bonds.

When more than one different conformations can exist in vacuo, calculations performed on Al surface showed different behaviours for the involved species. In particular, IQ would adsorb sensibly stronger if the intramolecular H-bond is broken, but the energy required for this process makes the most stable conformation to be adsorbed preferentially. On the other hand, the adsorption of QA occurs with the loss of the intramolecular H-bond and the same fate is shared by SA, even considering the huge energy difference between its two conformations: the breaking of intramolecular H-bond allows SA to form a very strong interaction network with the surface. Finally, in the MBI and MBT cases, where there is no intramolecular H-bond and the energy difference between the two conformations is small, the less stable form is the one with the stronger interaction; this because the SH group can participate as H-donor.

On the outer surface, the formation of H-bonds is hindered by steric repulsion or by the large energy difference between conformation with and without intramolecular hydrogen bond. As a result, all the investigate molecules adopt a parallel orientation with respect to the silicic surface, with an adsorption energy which, being of the order of the one calculated for benzene, is mainly due to weak dispersion forces. Sligthly larger adsorption energies are shown by MBI and MBT, likely due to an enanched interaction of the five-member ring with the surface.

The formation of aggregates between salicylaldoxime and quinaldic with HNT acid was characterized by thermogravimetric analysis and UV-VIS spectroscopy. The calculated net exoergicity (taking into account adsorption energy and conformational change energy) for QA and SA is -83.1 and -74.4 kJ mol^{-1}, respectively. This small difference hardly justifies the fact that, according to TGA experiment, QA loads in HNT with a much higher percentage. This evidence can be explained instead by considering that QA adsorbs on halloysite Al surface by forming multiple layer, this being in agreement with intermolecular interactions

that are stronger in QA than in SA, as results from DSC measurements and the Freundlich fit of UV-VIS adsorption isotherms.

Using different, larger models would be worthwile in future computational studies. This would allow the investigation of the adsorption of two or more molecules on the halloysite surface and their interactions with its interlayer.

Acknowledgement

The work was financially supported by Progetto di Ricerca e Sviluppo "AGM for CuHe" (ARS01_00697) and University of Palermo.

Supporting Information Available

The optimized geometries of all conformations and orientations of metal corrosion inhibitors adsorbed on the two surfaces of the Halloysite model. This material is available free of charge via the Internet at http://pubs.acs.org.

References

(1) Poznyak, S.; Tedim, J.; Rodrigues, L.; Salak, A.; Zheludkevich, M.; Dick, L.; Ferreira, M. Novel Inorganic Host Layered Double Hydroxides Intercalated with Guest Organic Inhibitors for Anticorrosion Applications. *ACS Appl. Mater. Interfaces* **2009**, *1*, 2353–2362.

(2) Abdullayev, E.; Price, R.; Shchukin, D.; Lvov, Y. Halloysite Tubes as Nanocontainers for Anticorrosion Coating with Benzotriazole. *ACS Appl. Mater. Interfaces* **2009**, *1*, 1437–1443.

(3) Twite, R.; Bierwagen, G. Review of Alternatives to Chromate for Corrosion Protection of Aluminum Aerospace Alloys. *Progr. Org. Coatings* **1998**, *33*, 91–100.

(4) Lutz, A.; van den Berg, O.; Van Damme, J.; Verheyen, K.; Bauters, E.; De Graeve, I.; Du Prez, F. E.; Terryn, H. A Shape-Recovery Polymer Coating for the Corrosion Protection of Metallic Surfaces. *ACS Appl. Mater. Interfaces* **2014**, *7*, 175–183.

(5) Stankiewicz, A.; Szczygieł, I.; Szczygieł, B. Self-Healing Coatings in Anti-Aorrosion Applications. *J. Mater. Sci.* **2013**, *48*, 8041–8051.

(6) Shchukin, D. G.; Möhwald, H. Surface-Engineered Nanocontainers for Entrapment of Corrosion Inhibitors. *Adv. Funct. Mater.* **2007**, *17*, 1451–1458.

(7) Montemor, M. et al. Evaluation of Self-Healing Ability in Protective Coatings Modified with Combinations of Layered Double Hydroxides and Cerium Molibdate Nanocontainers Filled with Corrosion Inhibitors. *Electrochimica Acta* **2012**, *60*, 31–40.

(8) Joshi, A.; Abdullayev, E.; Vasiliev, A.; Volkova, O.; Lvov, Y. Interfacial Modification of Clay Nanotubes for the Sustained Release of Corrosion Inhibitors. *Langmuir* **2012**, *29*, 7439–7448.

(9) Snihirova, D.; Lamaka, S.; Taryba, M.; Salak, A.; Kallip, S.; Zheludkevich, M.; Ferreira, M.; Montemor, M. Hydroxyapatite Microparticles as Feedback-Active Reservoirs of Corrosion Inhibitors. *ACS Appl. Mater. Interfaces* **2010**, *2*, 3011–3022.

(10) Balaskas, A.; Kartsonakis, I.; Tziveleka, L.-A.; Kordas, G. Improvement of Anti-Corrosive Properties of Epoxy-Coated AA 2024-T3 with TiO_2 Nanocontainers Loaded with 8-Hydroxyquinoline. *Progr. Org. Coatings* **2012**, *74*, 418–426.

(11) Lamaka, S. V.; Zheludkevich, M. L.; Yasakau, K.; Montemor, M.; Ferreira, M. G. High Effective Organic Corrosion Inhibitors for 2024 Aluminium Alloy. *Electrochimica Acta* **2007**, *52*, 7231–7247.

(12) Montemor, M. Functional and Smart Coatings for Corrosion Protection: A Review of Recent Advances. *Surf. Coat. Technol.* **2014**, *258*, 17–37.

(13) Zheng, Q.; Jiang, J.; Hou, D.; Wu, S.; Wang, F.; Yan, Y.; Sun, W. Formation and Structure of Inhibitive Molecular Film of Oxadiazole on Iron Surface. *J Phys. Chem. C* **2017**, *121*, 21420–21429.

(14) Cavallaro, G.; Lazzara, G.; Milioto, S.; Parisi, F.; Ruisi, F. Halloysite Nanotubes for Cleaning, Consolidation and Protection. *Chem. Record* **2018**, *18*, 940–949.

(15) Lazzara, G.; Cavallaro, G.; Panchal, A.; Fakhrullin, R.; Stavitskaya, A.; Vinokurov, V.; Lvov, Y. An Assembly of Organic-Inorganic Composites Using Halloysite Clay Nanotubes. *Curr. Opin. Colloid Interface Sci.* **2018**, *35*, 42–50.

(16) Lvov, Y.; Wang, W.; Zhang, L.; Fakhrullin, R. Halloysite Clay Nanotubes for Loading and Sustained Release of Functional Compounds. *Adv. Mater.* **2016**, *28*, 1227–1250.

(17) Lvov, Y. M.; DeVilliers, M. M.; Fakhrullin, R. F. The Application of Halloysite Tubule Nanoclay in Drug Delivery. *Expert Opinion on Drug Delivery* **2016**, *13*, 977–986.

(18) Tarasova, E.; Naumenko, E.; Rozhina, E.; Akhatova, F.; Fakhrullin, R. Cytocompatibility and Uptake of Polycations-Modified Halloysite Clay Nanotubes. *Appl. Clay Sci.* **2019**, *169*, 21–30.

(19) Cavallaro, G.; Chiappisi, L.; Pasbakhsh, P.; Gradzielski, M.; Lazzara, G. A Structural Comparison of Halloysite Nanotubes of Different Origin by Small-Angle Neutron Scattering (SANS) and Electric Birefringence. *Appl. Clay Sci.* **2018**, *160*, 71–80.

(20) Pasbakhsh, P.; Churchman, G. J.; Keeling, J. L. Characterisation of Properties of Various Halloysites Relevant to Their Use as Nanotubes and Microfibre Fillers. *Appl. Clay Sci.* **2013**, *74*, 47–57.

(21) Joussein, E.; Petit, S.; Churchman, J.; Theng, B.; Righi, D.; Delvaux, B. Halloysite Clay Minerals - A Review. *Clay Miner.* **2005**, *40*, 383–426.

(22) Yuan, P.; Tan, D.; Annabi-Bergaya, F. Properties and Applications of Halloysite Nanotubes: Recent Research Advances and Future Prospects. *Appl. Clay Sci.* **2015**, *112-113*, 75–93.

(23) Fakhrullin, R.; Tursunbayeva, A.; Portnov, V.; L'vov, Y. M. Ceramic Nanotubes for Polymer Composites with Stable Anticorrosion Properties. *Crystallography Rep.* **2014**, *59*, 1107–1113.

(24) Liu, F.; Bai, L.; Zhang, H.; Song, H.; Hu, L.; Wu, Y.; Ba, X. Smart H2O2-Responsive Drug Delivery System Made by Halloysite Nanotubes and Carbohydrate Polymers. *ACS Appl. Mater. Interfaces* **2017**, *9*, 31626–31633.

(25) Zhang, H.; Cheng, C.; Song, H.; Bai, L.; Cheng, Y.; Ba, X.; Wu, Y. A Facile One-Step Grafting of Polyphosphonium onto Halloysite Nanotubes Initiated by Ce(IV). *Chem. Commun.* **2019**, *55*, 1040–1043.

(26) Yah, W. O.; Xu, H.; Soejima, H.; Ma, W.; Lvov, Y.; Takahara, A. Biomimetic Dopamine Derivative for Selective Polymer Modification of Halloysite Nanotube Lumen. *J. Am. Chem. Soc.* **2012**, *134*, 12134–12137.

(27) Lvov, Y. M.; Shchukin, D. G.; Mohwald, H.; Price, R. R. Halloysite Clay Nanotubes for Controlled Release of Protective Agents. *ACS Nano* **2008**, *2*, 814–820.

(28) Abdullayev, E.; Abbasov, V.; Tursunbayeva, A.; Portnov, V.; Ibrahimov, H.; Mukhtarova, G.; Lvov, Y. Self-Healing Coatings Based on Halloysite Clay Polymer Composites for Protection of Copper Alloys. *ACS Appl. Mater. Interfaces* **2013**, *5*, 4464–4471.

(29) Abdullayev, E.; Lvov, Y. Halloysite Clay Nanotubes for Controlled Release of Protective Agents. *J. Nanosci. Nanotechnol.* **2011**, *11*, 10007–10026.

(30) Abdullayev, E.; Lvov, Y. Clay Nanotubes for Corrosion Inhibitor Encapsulation: Release Control with End Stoppers. *J. Mater. Chem.* **2010**, *20*, 6681–6687.

(31) Frisch, M. J. et al. Gaussian 09 Revision D.01. Gaussian Inc. Wallingford CT 2009.

(32) Zhao, Y.; Truhlar, D. G. A New Local Density Functional for Main-Group Thermochemistry, Transition Metal Bonding, Thermochemical Kinetics, and Noncovalent Interactions. *J. Chem. Phys.* **2006**, *125*, 194101.

(33) Schaefer, A.; Horn, H.; Ahlrichs, R. Fully Optimized Contracted Gaussian-Basis Sets for Atoms Li to Kr. *J. Chem. Phys.* **1992**, *97*, 2571–2577.

(34) Eichkorn, K.; Treutler, O.; Ohm, H.; Haser, M.; Ahlrichs, R. Auxiliary Basis-Sets to Approximate Coulomb Potentials. *Chem. Phys. Lett.* **1995**, *240*, 283–289.

(35) Eichkorn, K.; Weigend, F.; Treutler, O.; Ahlrichs, R. Auxiliary Basis Sets for Main Row Atoms and Transition Metals and Their Use to Approximate Coulomb Potentials. *Theor. Chem. Acc.* **1997**, *97*, 119–124.

(36) Ferrante, F.; Armata, N.; Lazzara, G. Modeling of the Halloysite Spiral Nanotube. *J. Phys. Chem. C* **2015**, *119*, 16700–16707.

(37) Ferrante, F.; Armata, N.; Cavallaro, G.; Lazzara, G. Adsorption Studies of Molecules on the Halloysite Surfaces: A Computational and Experimental Investigation. *J. Phys. Chem. C* **2017**, *121*, 2951–2958.

(38) Boys, S.; Bernardi, F. The Calculation of Small Molecular Interactions by the Differences of Separate Total Energies. Some Procedures with Reduced Errors. *Mol. Phys.* **1970**, *19*, 553–566.

(39) Sciascia, L.; Casella, S.; Cavallaro, G.; Lazzara, G.; Milioto, S.; Princivalle, F.; Parisi, F. Olive Mill Wastewaters Decontamination Based on Organo-nano-clay Composites. *Ceramics International* **2019**, *45*, 2751 – 2759.

(40) Cavallaro, G.; Lazzara, G.; Milioto, S.; Parisi, F.; Ruisi, F. Nanocomposites Based on Esterified Colophony and Halloysite Clay Nanotubes as Consolidants for Waterlogged Archaeological Woods. *Cellulose* **2017**, *24*, 3367–3376.

(41) De Lisi, R.; Lazzara, G.; Milioto, S.; Muratore, N. Laponite Clay in Homopolymer and Tri-block Copolymer Matrices. *J. Thermal Anal. Calorim.* **2007**, *87*, 61–67.

(42) Malakhov, D. V.; Abou Khatwa, M. K. Constructing a Self-Consistent Integral Baseline by Using Cubic Splines. *J. Thermal Anal. Calorim.* **2007**, *87*, 595–599.

(43) Duce, C.; Vecchio Ciprioti, S.; Ghezzi, L.; Ierardi, V.; Tinè, M. Thermal Behavior Study of Pristine and Modified Halloysite Nanotubes. *J. Therm. Anal. Calorim.* **2015**, *121*, 1011–1019.

(44) Calabrese, I.; Cavallaro, G.; Lazzara, G.; Merli, M.; Sciascia, L.; Turco Liveri, M. L. Preparation and Characterization of Bio-Organoclays Using Nonionic Surfactant. *Adsorption* **2016**, *22*, 105–116.

(45) Cavallaro, G.; Lazzara, G.; Milioto, S.; Parisi, F.; Sanzillo, V. Modified Halloysite Nanotubes: Nanoarchitectures for Enhancing the Capture of Oils from Vapor and Liquid Phases. *ACS Appl. Mater. Interfaces* **2014**, *6*, 606–612.

(46) Hatch, C. D.; Wiese, J. S.; Crane, C. C.; Harris, K. J.; Kloss, H. G.; Baltrusaitis, J. Water Adsorption on Clay Minerals As a Function of Relative Humidity: Application of BET and Freundlich Adsorption Models. *Langmuir* **2012**, *28*, 1790–1803.

(47) Sá, A. D.; Abreu, A. S.; Moura, I.; Machado, A. V. In *Water Purification*; Grumezescu, A. M., Ed.; Academic Press, 2017; pp 289 – 322.

(48) Ma, Y. et al. Porous Lignin Based Poly-(Acrylic Acid)/Organo-Montmorillonite Nanocomposites: Swelling Behaviors and Rapid Removal of Pb(II) Ions. *Polymer* **2017**, *128*, 12 – 23.

(49) Sathishkumar, P.; Arulkumar, M.; Ashokkumar, V.; Mohd Yusoff, A. R.; Murugesan, K.; Palvannan, T.; Salam, Z.; Ani, F. N.; Hadibarata, T. Modified Phyto-waste Terminalia Catappa Fruit Shells: a Reusable Adsorbent for the Removal of Micropollutant Diclofenac. *RSC Adv.* **2015**, *5*, 30950–30962.

(50) Han, G.; Huang, Y.; Li, G.; Zhang, Y.; Jiang, T. Detailed Adsorption Studies of Active Humic Acid Fraction of a New Binder on Iron Ore Particles. *Min. Proc. Ext. Met. Rev.* **2014**, *35*, 1–14.

(51) Buttini, F.; Soltani, A.; Colombo, P.; Marriott, C.; Jones, S. Multilayer PVA Adsorption onto Hydrophobic Drug Substrates to Engineer Drug-rich Microparticles. *Eur. J. Pharm. Sci.* **2008**, *33*, 20 – 28.

(52) Santosa, S. J.; Siswanta, D.; Kurniawan, A.; Rahmanto, W. H. Hybrid of Chitin and Humic Acid as High Performance Sorbent for Ni(II). *Surf. Sci.* **2007**, *601*, 5155 – 5161.

(53) Chen, Z.; Xing, B.; McGill, W. B. A Unified Sorption Variable for Environmental Applications of the Freundlich Equation. *J. Environ. Quality* **1999**, *28*, 1422–1428.

Table 1: The BSSE-corrected interaction energies of the selected corrosion inhibitors adsorbed on the halloysite silicic surface. Letters a, b and c are the labels for molecular conformations; pl and pp indicate the parallel or perpendicular orientation of the molecule with respect to surface in the starting geometry.

	ΔE_{ads} / kJ mol^{-1}		
	a	**b**	**c**
pl BT	−23.2		
pp BT	−20.4		
pl IQ	−25.5	−24.4	
pp IQ	−21.5	−13.0	
pl MBI	−33.6	−10.8	
pp MBI	−38.9	−21.6	
pl MBT	−26.8	−21.7	
pp MBT	−30.8	−21.0	
pl QA	−26.6	−31.6	−28.3
pp QA	−22.2	−11.8	−16.6
pl SA	−28.2	−26.2	
pp SA	−23.0	−13.0	

Table 2: The BSSE-corrected interaction energies of the selected corrosion inhibitors adsorbed on the halloysite aluminic surface. Letters a, b and c are the labels for molecular conformations; pl and pp indicate the parallel or perpendicular orientation of the molecule with respect to surface in the starting geometry.

	ΔE_{ads} / kJ mol^{-1}		
	a	**b**	**c**
pl BT	−59.5		
pp BT	−62.3		
pl IQ	−72.4	−37.4	
pp IQ	−78.5	−56.4	
pl MBI	−67.6	−46.2	
pp MBI	−92.5	−58.1	
pl MBT	−55.1	−44.6	
pp MBT	−74.0	−38.9	
pl QA	−99.0	−69.8	−77.9
pp QA	−80.0	−76.4	−99.0
pl SA	−110.1	−54.1	
pp SA	−117.3	−69.9	

Table 3: Sorption parameters of the Freundlich model for the adsorption isotherms of QA and SA onto HNT clay. K_F is expressed in mg g^{-1} $(dm^3\ g^{-1})^{1/n}$.

	QA	**SA**
K_F	20.4±0.9	4.4±0.5
n	2.15±0.09	3.0±0.5
R^2	0.987	0.904

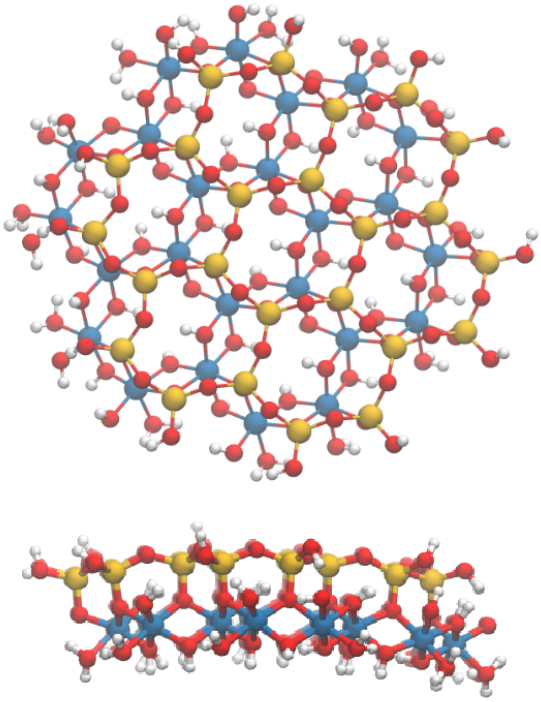

Figure 1: The $H_{48}Al_{24}Si_{24}O_{126}$ portion of halloysite nanotube used for adsorption studies. Atom colors are: white for H, red for O, yellow for Si and light blue for Al.

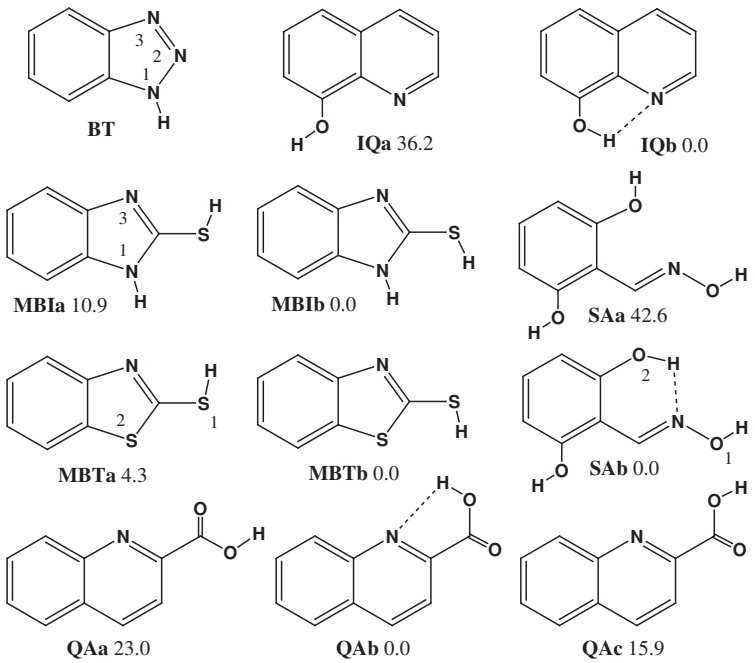

Figure 2: The considered conformations for the corrosion inhibitors investigated in this work. Reported energies (in kJ mol^{-1}) are referred to the most stable form.

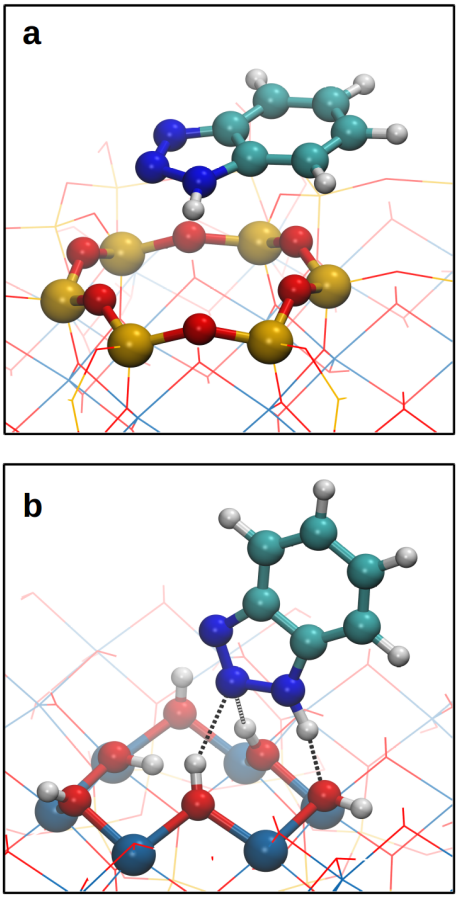

Figure 3: The adsorption geometry of the benzotriazole molecule on (a) silicic and (b) aluminic surface [H-bonds parameters: NH-O(1.664, 167), N_2-HO(2.199, 158/2.147, 152)] of the halloysite model.

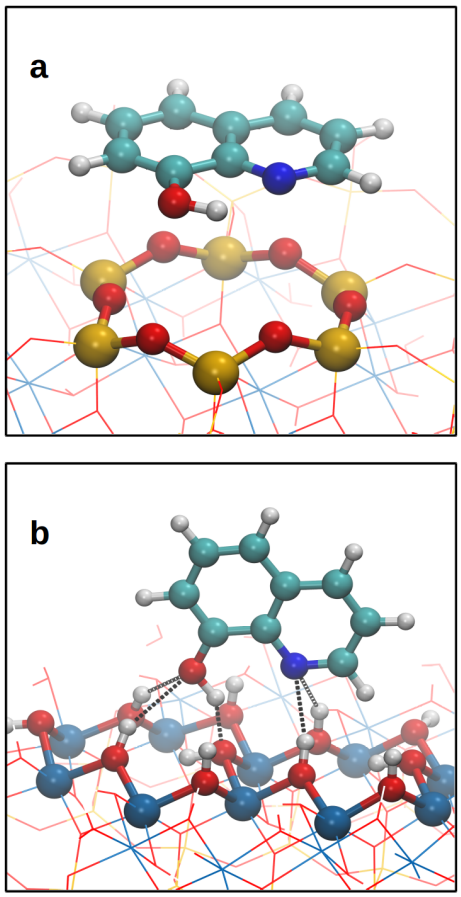

Figure 4: The adsorption geometry of the 8-hydroxyquinoline molecule on (a) silicic and (b) aluminic surface [H-bonds parameters: OH-O(1.662, 147), O-HO(2.238, 154/2.496, 150), N-HO(2.321, 157/2.430, 143)] of the halloysite model.

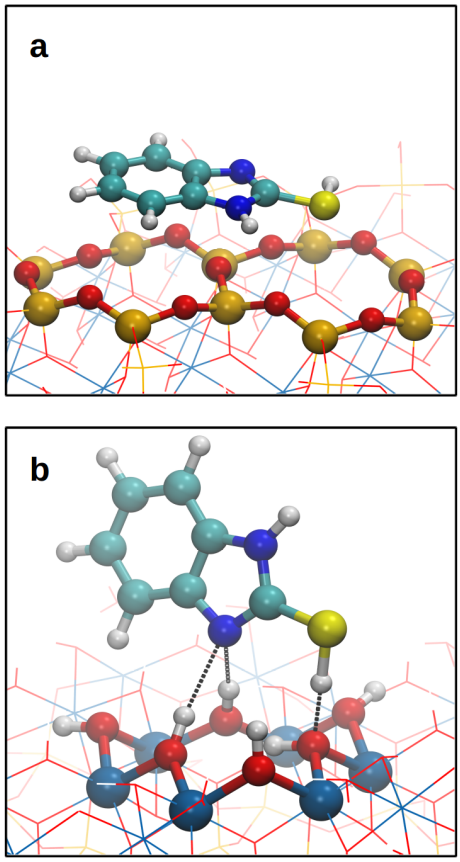

Figure 5: The adsorption geometry of the 2-mercaptobenzimidazole molecule on (a) silicic and (b) aluminic surface [H-bond parameters: N-HO(2.025, 172/2.453, 167), SH-O(1.656, 178)] of the halloysite model.

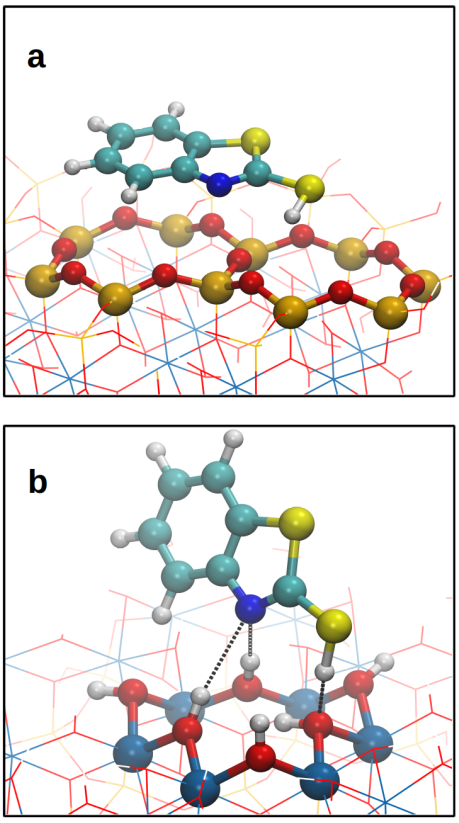

Figure 6: The adsorption geometry of the 2-mercaptobenzothiazole molecule on (a) silicic and (b) aluminic surface [H-bond parameters: N-HO(2.105, 175/2.649, 163), SH-O(1.669, 175)] of the halloysite model.

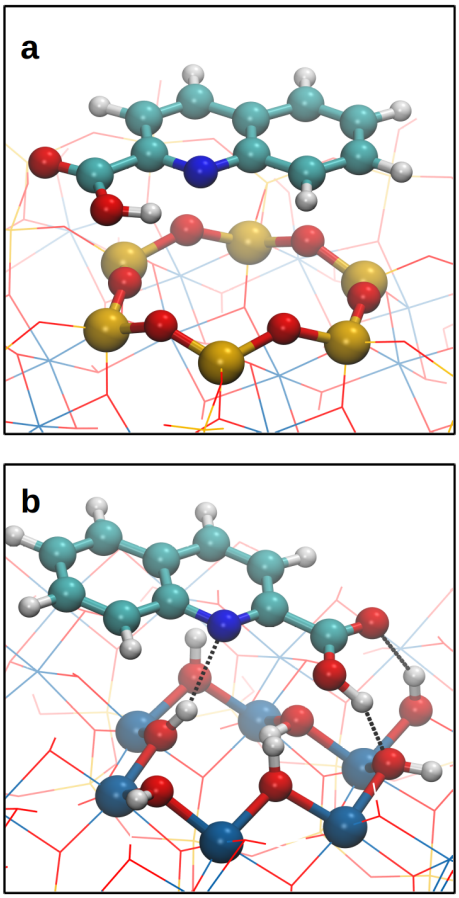

Figure 7: The adsorption geometry of the quinaldic acid molecule on (a) silicic and (b) aluminic surface [H-bond parameters: OH-O(1.711, 153), O-HO(1.963, 152), N-HO(2.201, 149)] of the halloysite model.

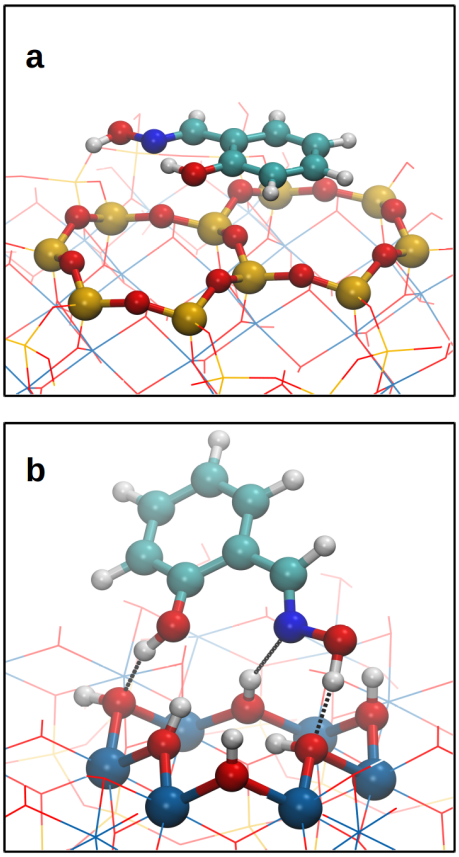

Figure 8: The adsorption geometry of the salicylaldoxime molecule on (a) silicic and (b) aluminic surface [H-bond parameters: OH-O(1.712, 159), OH-O(1.617, 160), N-HO(2.100, 157)] of the halloysite model.

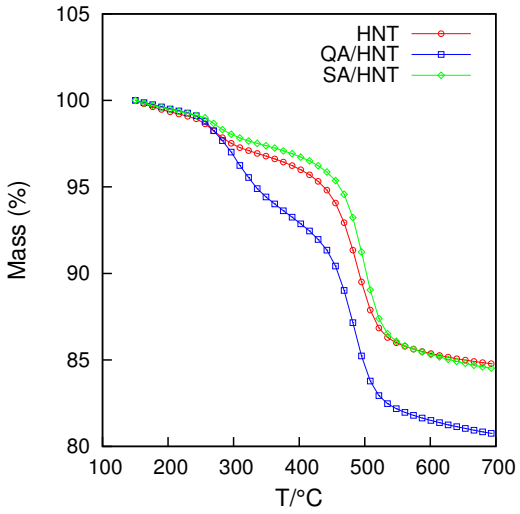

Figure 9: Thermogravimetric curves for pristine HNT, QA/HNT and SA/HNT.

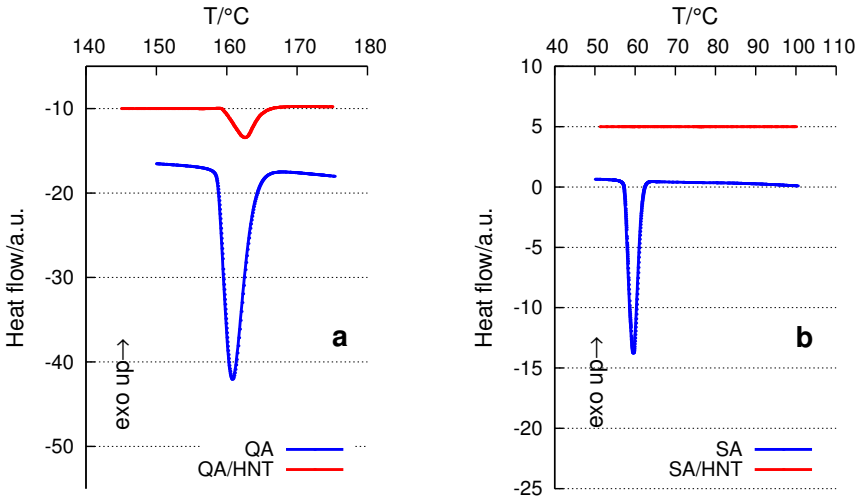

Figure 10: Differential scanning calorimetry curves for pure QA and SA, and their composites with HNT.

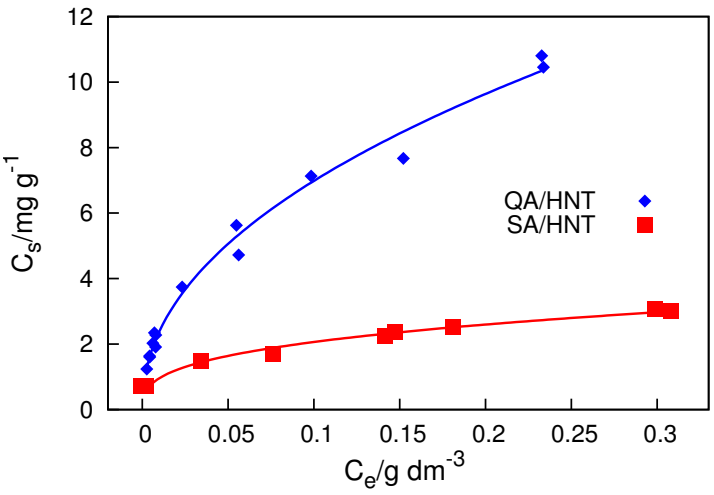

Figure 11: Adsorption isotherms of QA and SA onto HNT. Symbols denote experimental points; lines correspond to the fit by Freundlich model.

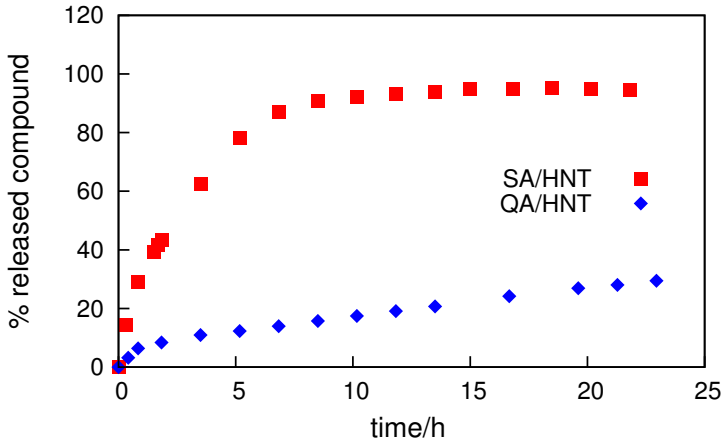

Figure 12: Kinetics of salicylaldoxime and quinaldic acid released from SA/HNT and QA/HNT.

TOC Graphic